VITAL SIGNS FROM INSIDE A HELMET: A MULTICHANNEL FACE-LEAD STUDY

Wilhelm von Rosenberg, Theerasak Chanwimalueang*, David Looney, Danilo P. Mandic*

Imperial College London
Electrical and Electronic Engineering
{wilhelm.von-rosenberg12, tc2113, david.looney06, d.mandic}@imperial.ac.uk

ABSTRACT

It is essential to measure physiological parameters such as heart rate variability and respiratory rate of drivers to evaluate their performance. The results from this measurement can be used to assess the state of body and mind, for instance concentration and stress. However, current systems only work in controlled environments, or sensors obstruct and interfere with operations of the driver. In this study, a face-lead ECG is placed inside a helmet to enhance comfort and convenience in racing scenarios. Multiple electrodes were attached to facial locations, which exhibit good contact with a helmet, and bipolar configurations were examined between the left and right side of the subject's face. Standard and data-driven filtering algorithms were employed to improve the extraction of R peaks from the ECG data. The so-extracted R peaks were subsequently used to estimate heart activity and respiration effort, and the results were compared with standard recording protocols. It is shown that ECG recordings obtained from locations on the lower jaw match closely with conventional recording paradigms (limb-lead ECG), highlighting the potential of vital sign monitoring from within a racing helmet.

Index Terms— Electrocardiogram ECG, vital signs, racing helmet, respiratory rate, MEMD.

1. INTRODUCTION

In motor car and motorcycle racing, the performance of drivers depends on many factors, such as driving skill, emotion, pathology and health. Inside a racing car or on a motorcycle, a driver is subjected to different levels of psychological stress which can impact performance. The relevant signatures of stress are contained in physiological parameters, such as heart, respiratory or brain function. For instance, the cardiac parameters of a Formula One driver were investigated in [1] with a limb-lead electrocardiogram (ECG) configuration placed at the arms, and it was shown that the correlation between the car velocity and heart rate was positively linear. In many racing scenarios, however, standard recording configurations are not practical as they are uncomfortable and can hinder performance, thus highlighting the need for wearable and unobtrusive platforms for recording vital signs [2].

The aim of this study is to examine the potential of ECG recordings from face locations inside a helmet, referred to as the face-lead ECG, in monitoring both cardiac and respiratory function. Advantages of the proposed approach are: (i) the enhanced comfort and convenience in racing scenarios compared with standard limb configurations; and (ii) improved fidelity of the recorded data, due to the good contact between the electrodes and skin, compared with head-based systems without helmet support.

Various approaches for recording cardiac activity at head-based locations have recently been introduced. A behind-the-ear approach, using a ballistocardiographic sensor and a single lead ECG configuration, was proposed by [3, 4] where it was illustrated that the recordings exhibited significantly more noise than those obtained from conventional recording configurations, at e.g. the arm, but that the relevant peak information could be extracted. Vital sign recordings of ECG and electrooculogram (EOG) from within a military helmet were examined in [5, 6] and compared with conventional recording configurations, however, only two electrode positions located on the forehead, attached by a sweatband, and the jaw, attached by a strap, were studied.

We propose to investigate five face locations which exhibit good skin contact due to helmet support. The face-lead configuration is located approximately between lead I and lead III [7], but currents travel a larger distance from the heart and through inhomogeneous tissues of irregular geometries, so that the recorded data is likely to be contaminated by artifacts from the head, such as eye blinking, brain activity, and jaw and cheek movements. To process face-lead signals, we used the multivariate empirical mode decomposition (MEMD) [8, 9], a recursive nonlinear filter which is suitable for multichannel and nonstationary data. The intrinsic patterns of these signals can be extracted using MEMD to separate the underlying cardiac data from artifacts [10]. Furthermore, following recent research by [11, 12, 13], the MEMD approach was used to extract respiratory effort form the face-lead recording.

*these authors contributed equally to this work

Fig. 1: The standard limb-lead ECG, respiratory signal and face-lead setup (top-left). The subject wearing a racing helmet with the face-lead configuration (above-right). Electrodes were attached to five locations on the face, the zygomatic bone, frontal bone, angle of mandible, body of mandible and lower mandible (lower).

2. THE MEMD ALGORITHM

The original empirical mode decomposition (EMD) algorithm [14] is a recursive nonlinear filter which decomposes a time series into a set of narrow-band scales known as intrinsic mode functions (IMFs). The properties of the IMFs are such that they enable a localised time-frequency representation by the Hilbert transform.

The multivariate extension [8, 9], see Algorithm 1, facilitates an enhanced operation for multi-channel data. In noise-assisted MEMD (NA-MEMD), additional channels containing white Gaussian noise (WGN) with a specified signal-to-noise ratio are created. This reduces unwanted phenomena in the 'signal-IMF' channels such as mode-mixing, see [15, 16] for details, and enables a more accurate estimation of IMFs in the presence of noise.

3. EXPERIMENTAL PROTOCOL

Gold cup electrodes were attached to 5 locations on the face: frontal bone (FB), zygomatic bone (ZB), angle of mandible (AM), body of mandible (BM), and lower mandible (LM) as shown Fig. 1. These locations were selected based on the areas where the helmet makes good contact with the skin. One exception is the lower mandible location where the jaw strap was used to attach the electrodes. An additional signal (AV) is created by averaging the three channels around the lower mandible (AM, BM, and LM). A bipolar configuration was set-up between the left and right side of the face of the subject. The centre of the forehead served as the common ground. The standard limb-lead III (left and right arm lead), and the respiratory signal, measured by piezo-electric sensor, were used as reference signals. A conductive gel was applied to reduce the impedance between skin and all electrodes. After attaching the electrodes, the subject was instructed to wear the helmet as shown in Fig. 1. Avatar EEG, a bio-amplifier manufactured by EGI, was used to record the face-lead signals. The sampling frequency was set to 500 Hz, and locations of the electrodes were unobtrusive to the eye and nose areas. The subject sat comfortably on a chair without moving for a recording duration of 3 minutes.

Algorithm 1 Multivariate EMD (MEMD)

Input: $\mathbf{V}(t) = [v^1(t), v^2(t), \ldots, v^N(t)]^T$

1. Create a suitable set of points on an (N-1) sphere for weighting: $\mathbf{w}_k = \{w_{\{k,1\}}, w_{\{k,2\}}, \ldots, w_{\{k,N\}}\}_{k=1}^K$, where K is the number of projections;
2. Along each vector $\mathbf{w}_k$, calculate a projection, denoted by $\rho\left(\mathbf{V}(t)\right)^{\mathbf{w}_k}$, of the input signal $\mathbf{V}(t)$ for all k, giving $\{\rho\left(\mathbf{V}(t)\right)^{\mathbf{w}_k}\}_{k=1}^K$ as the set of projections;
3. Identify the time instants $\{t_j^{\mathbf{w}_k}\}$ of the maxima (and minima) of the set of projections;
4. Compute the multivariate maxima (and minima) envelope curves $\{\epsilon_{\max}^{\mathbf{w}_k}(t)\}_{k=1}^K$ (and $\{\epsilon_{\max}^{\mathbf{w}_k}(t)\}_{k=1}^K$) by interpolating $[t_j^{\mathbf{w}_k}, \mathbf{V}(t_j^{\mathbf{w}_k})]$;
5. The mean $\mathbf{m}(t)$ of the envelope curves of a set of K direction vectors is calculated as:
$$\mathbf{m}(t) = \frac{1}{2K}\sum_{k=1}^{K} \epsilon_{\max}^{\mathbf{w}_k}(t) + \epsilon_{\min}^{\mathbf{w}_k}(t)$$
6. The 'detail' $\hat{\mathbf{g}}$ is defined as: $\hat{\mathbf{g}} = \mathbf{V}(t) - \mathbf{m}(t)$. If it fulfills the stoppage criterion for a multivariate IMF, apply the above procedure to $\mathbf{V}(t) - \hat{\mathbf{g}}(t)$; if not, apply it to $\hat{\mathbf{g}}(t)$.

4. FACE-LEAD ANALYSIS

The raw data from the five channels (respiration and arm ECG were for reference only) were processed in three offline steps as shown in Fig. 2: (i) the multichannel signal was filtered using a Butterworth bandpass filter (BPF), MEMD and NA-MEMD; (ii) R peaks (the most dominant feature in the ECG cycle) were identified; and (iii) the respiration estimated

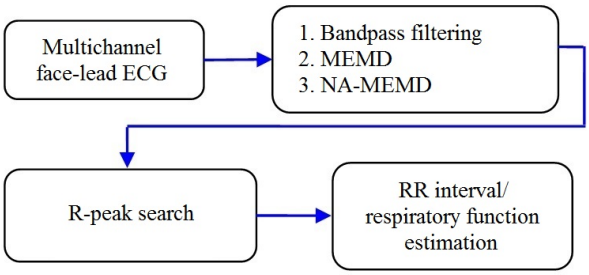

Fig. 2: The processing steps in the identification of heart and respiratory function.

from the RR intervals. A total of 64 projection direction were taken for both MEMD and NA-MEMD. For NA-MEMD, 20 realisations of five channels of WGN at 20 dBm were generated and averaged across the individual IMFs. The noise power was scaled based on the power of one of the face-lead channels, the lower mandible. For MEMD and NA-MEMD, a linear weighting was applied to the IMFs to obtain the desired output frequency range. The weights were obtained using a time-frequency binary-mask approach supported by the Wiener filter (see [17] for details).

For all approaches the optimal frequency range was determined by comparing the number of correctly identified R peaks obtained within a frequency range between f_{min} and f_{max}, where f_{min} can have all integer values from 1 to 20 and f_{max} all integer values from 6 to 40 with the condition that $f_{max} - f_{min} > 4$. Thus, a total of 510 frequency ranges were considered.

The R peak search was achieved by identifying local peaks in the signal amplitudes above a certain threshold and with a minimum separation in time. The RR intervals, the time between two adjacent R peaks, were calculated for all three filtering methods and used to estimate the respiration signal using cubic spline interpolation. The respiration function can be obtained from ECG for subjects that exhibit the phenomenon of respiratory sinus arrhythmia (RSA) [18, 19, 20, 21].

5. RESULTS

The results of the different filtering operations for recordings obtained from the LM location are shown in Fig. 3, the ECG obtained from the arm is also shown. The positions of the detected R peaks are marked with crosses. An R peak is said to be correctly identified when its position is within a certain interval before or after the peak in the reference ECG. For empirical reasons, this interval is defined as 2% of the average time difference between two adjacent heart beats. Table 1 displays the number of correct and incorrect peak identifications for the five bipolar electrode arrangements, and an average of the three most accurate ones (AV) using the three

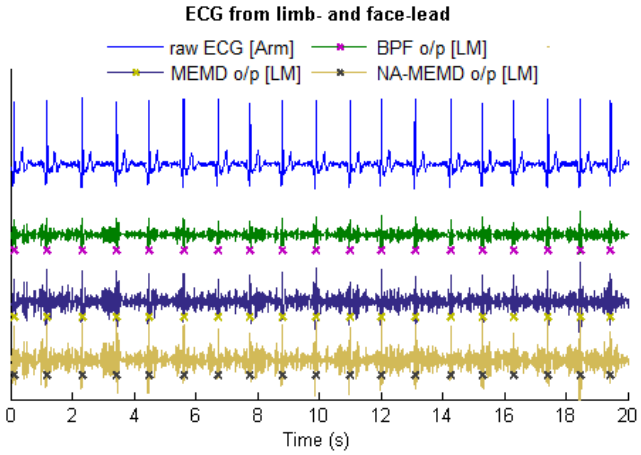

Fig. 3: Signal and detected peaks (crosses) after applying the methods BPF, MEMD, and NA-MEMD to measurements at the LM collated with limb-lead ECG.

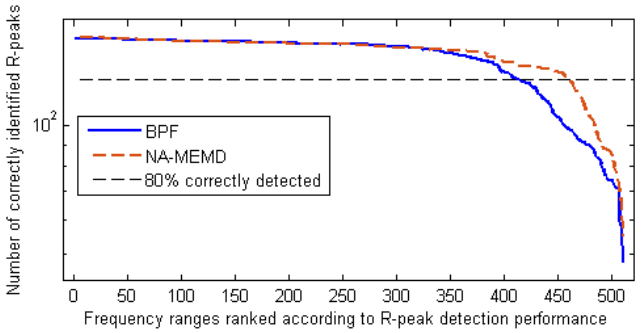

Fig. 4: Performance of the frequency ranges sorted according to their accuracy in detecting R peaks correctly (displayed here for AV, similar graphs for AM, BM, and LM).

filtering approaches (BPF, MEMD, and NA-MEMD).

Fig. 4 illustrates the performance of all investigated frequency ranges. The number of correctly identified R peaks of the most reliable ranges for BPF and NA-MEMD match, but

Table 1: Left: Number of correctly identified R peaks at five electrode locations after: (a) BPF, (b) MEMD, and (c) NA-MEMD. The reference arm ECG identified 160 peaks in total. Right: Number of frequency ranges per approach that detect at least 80% of the R peaks.

Electrode location	Correctly identified peaks (out of 160)			Number of freq. ranges with success rate >80%		
	(a)	(b)	(c)	(a)	(b)	(c)
1) FB	18	17	17	0	0	0
2) AM	157	152	157	340	356	371
3) BM	159	157	160	375	401	443
4) LM	129	159	159	370	397	400
5) ZB	86	79	83	0	0	0
6) AV	159	158	160	413	420	460

Table 2: The heart rate derived from detected peaks at five locations compared to the true heart rate (mean (μ)=56.6 beats per minute (bpm), standard deviation (σ): 1.4 bpm). The deviation is calculated at 148 points in time.

Electrode location	Peak rate (in bpm, arm ECG: 56.6) $\mu \pm \sigma$			Deviation from the heart rate (in bpm) $\mu \pm \sigma$		
	BPF	MEMD	NA-MEMD	BPF	MEMD	NA-MEMD
1) Frontal bone	79.1±4.1	77.3±4.4	70.2±6.5	22.2±3.9	20.6±4.7	13.2±6.6
2) Angle of mandible	56.6±1.5	56.6±1.6	56.6±1.5	<0.05±0.2	<0.05±0.3	<0.05±0.1
3) Body of mandible	56.6±1.5	56.6±1.5	56.6±1.4	<0.05±0.1	<0.05±0.1	<0.05±0.1
4) Lower mandible	56.6±1.4	56.6±1.4	56.6±1.4	<0.05±0.1	<0.05±0.1	<0.05±0.1
5) Zygomatic bone	61.1±3.6	61.7±4.3	64.7±4.3	4.3±4.0	5.1±4.4	8.1±4.8
6) Avg. of (2) to (4)	56.6±1.5	56.6±1.4	56.6±1.5	<0.05±0.1	<0.05±0.1	<0.05±0.1

more frequency ranges for NA-MEMD detect at least 80% of the peaks, highlighting how the approach is less dependent on the choice of parameters (f_{max} and f_{min}).

The three locations on the lower jaw and their average signal have the highest success rate while the results of the other two locations indicate high noise levels. Extracted peaks were utilised to obtain the heart rate from sliding windows comprising 11 consecutive peaks. Table 2 summarises the results and furthermore contains the deviation of the calculated heart rate from the actual heart rate, which was simultaneously obtained from the reference arm ECG. Since this is based on previous results, the same three locations lead to the most reliable values where signals after bandpass filtering, MEMD, and NA-MEMD all lead to an accurate estimation of the heart rate (the mean is is in accordance with the actual value and the deviation from the real rate is small over the whole period).

In the next step, the temporal distances between adjacent peaks, the RR intervals, were obtained to detect the respiratory rate via the phenomenon of RSA. Fig. 5 displays the respiration recorded by the respiration belt compared to the dynamics of the RR intervals over time measured at the lower mandible. In this case, and for the angle and body of mandible, an explicit correlation between the respiration belt and the RR intervals was found.

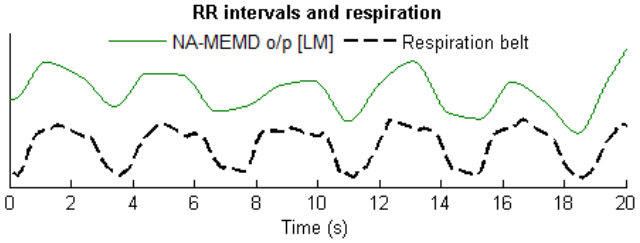

Fig. 5: The dynamics of RR intervals over time obtained from the LM compared with respiration (lower). (The graphs for AM, BM, and AV are approximately identical.)

6. CONCLUSION

We have illuminated conclusively that it is possible to extract the heart rate from electrodes attached to facial locations which are convenient and comfortable when wearing a helmet. This has been achieved by applying bandpass filtering, MEMD and NA-MEMD to the recorded signals. Out of the five examined locations, the most accurate for R peak detection are the three around the lower jaw. Comparing the three different filtering methods, bandpass filtering and NA-MEMD achieve similarly good results. However, more frequency ranges for NA-MEMD detect at least 80% of the R peaks, i.e. it is expected to be more robust to different environments and subjects, see Fig. 4 and Table 1.

We have also demonstrated that face-lead ECG admits the detection of respiration effort from the RR intervals. This has highlighted the value of recording vital signs from the inside of a helmet. Future work will examine real-life driving situations, alternative sensor technologies, different types of helmets and will combine our existing work with recordings from the brain.

7. REFERENCES

[1] R. Bedini, A. Belardinelli, G. Palagi, M. Varanini, A. Ripoli, S. Berti, C. Carpeggiani, F. Paone, and R. Ceccarelli, "ECG telemetric evaluation in Formula One drivers," in *Proceedings of the IEEE International Conference on Computers in Cardiology*, 1995, pp. 353–356.

[2] P. Bonato, "Wearable sensors and systems," *IEEE Engineering in Medicine and Biology Magazine*, vol. 29, no. 3, pp. 25–36, 2010.

[3] D. Da He, E. S. Winokur, and C. G. Sodini, "A continuous, wearable, and wireless heart monitor using head ballistocardiogram (BCG) and head electrocardiogram (ECG)," in *Proceedings of the IEEE International Conference on Engineering in Medicine and Biology Society (EMBC)*, 2011, pp. 4729–4732.

[4] D. Da He, E. S. Winokur, T. Heldt, and C. G. Sodini, "The ear as a location for wearable vital signs monitoring," in *Proceedings of the IEEE International Conference on Engineering in Medicine and Biology Society (EMBC)*, 2010, pp. 6389–6392.

[5] Y. S. Kim, H. B. Lee, J. S. Kim, H. J. Baek, M. S. Ryu, and K. S. Park, "ECG, EOG detection from helmet based system," in *Proceedings of the IEEE International Conference on Information Technology Applications in Biomedicine (ITAB)*, 2007, pp. 191–193.

[6] Y. S. Kim, J. M. Choi, H. B. Lee, J. S. Kim, H. J. Baek, M. S. Ryu, R. H. Son, and K. S. Park, "Measurement of biomedical signals from helmet based system," in *Proceedings of the IEEE International Conference on Engineering in Medicine and Biology Society (EMBS)*, 2007, pp. 359–362.

[7] T. Shen, T. Hsiao, Y. Liu, and T. He, "An ear-lead ECG based smart sensor system with voice biofeedback for daily activity monitoring," in *Proceedings of the IEEE International Region 10 Conference (TENCON)*, 2008, pp. 1–6.

[8] N. Ur Rehman and D. P. Mandic, "Multivariate empirical mode decomposition," *Proceedings of the Royal Society A: Mathematical, Physical and Engineering Sciences*, vol. 466, no. 2117, pp. 1291–1302, 2010.

[9] D. P. Mandic, N. Ur Rehman, Z. Wu, and N. E. Huang, "Empirical mode decomposition-based time-frequency analysis of multivariate signals: The power of adaptive data analysis," *IEEE Signal Processing Magazine*, vol. 30, no. 6, pp. 74–86, 2013.

[10] K. J. Lee and B. Lee, "Removing ECG artifacts from the EMG: A comparison between combining empirical-mode decomposition and independent component analysis and other filtering methods," in *Proceedings of the IEEE International Conference on Control, Automation and Systems (ICCAS)*, 2013, pp. 181–184.

[11] M. Campolo, D. Labate, F. La Foresta, F. C. Morabito, A. Lay-Ekuakille, and P. Vergallo, "ECG-derived respiratory signal using empirical mode decomposition," in *Proceedings of the International IEEE Workshop on Medical Measurements and Applications (MeMeA)*, 2011, pp. 399–403.

[12] D. Labate, F. L. Foresta, G. Occhiuto, F. C. Morabito, A. Lay-Ekuakille, and P. Vergallo, "Empirical mode decomposition vs. wavelet decomposition for the extraction of respiratory signal from single-channel ECG: A comparison," *IEEE Sensors Journal*, vol. 13, no. 7, pp. 2666–2674, 2013.

[13] R. Mabrouki, B. Khaddoumi, and M. Sayadi, "R peak detection in electrocardiogram signal based on a combination between empirical mode decomposition and Hilbert transform," in *Proceedings of the IEEE International Conference on Advanced Technologies for Signal and Image Processing (ATSIP)*, 2014, pp. 183–187.

[14] N. E. Huang, Z. Shen, S. R. Long, M. C. Wu, H. H. Shih, Q. Zheng, N.-C. Yen, C. C. Tung, and H. H. Liu, "The empirical mode decomposition and the Hilbert spectrum for nonlinear and non-stationary time series analysis," *Proceedings of the Royal Society A: Mathematical, Physical and Engineering Sciences*, vol. 454, no. 1971, pp. 903–995, 1998.

[15] N. Ur Rehman and D. P. Mandic, "Filter bank property of multivariate empirical mode decomposition," *IEEE Transactions on Signal Processing*, vol. 59, no. 5, pp. 2421–2426, 2011.

[16] N. Ur Rehman, C. Park, N. E. Huang, and D. P. Mandic, "EMD via MEMD: Multivariate noise-aided computation of standard EMD," *Advances in Adaptive Data Analysis*, vol. 5, no. 2, pp. 1350007 (1–25), 2013.

[17] D Looney, L. Li, T. M. Rutkowski, D. P. Mandic, and A. Cichocki, "Ocular artifacts removal from EEG using EMD," in *Advances in Cognitive Neurodynamics ICCN*, pp. 831–835. Springer, 2008, 00023.

[18] C. Orphanidou, S. Fleming, S. A. Shah, and L. Tarassenko, "Data fusion for estimating respiratory rate from a single-lead ECG," *Biomedical Signal Processing and Control*, vol. 8, no. 1, pp. 98–105, 2013.

[19] V. Goverdovsky, D. Looney, P. Kidmose, C. Papavassiliou, and D. P. Mandic, "Co-located multimodal sensing: A robust solution for next generation wearable health," *IEEE Sensors Journal*, vol. 15, no. 1, pp. 138–145, 2015.

[20] K. V. Madhav, M. R. Ram, E. H. Krishna, N. R. Komalla, and K. A. Reddy, "Estimation of respiration rate from ECG, BP and PPG signals using empirical mode decomposition," in *Proceedings of the IEEE International Instrumentation and Measurement Technology Conference (I2MTC)*, 2011, pp. 1–4.

[21] E. J. Bowers, A. Murray, and P. Langley, "Respiratory rate derived from principal component analysis of single lead electrocardiogram," in *Proceedings of the IEEE International Conference on Computers in Cardiology*, 2008, pp. 437–440.